**Journal of Materials Science and Engineering with Advanced Technology**
Volume 8, Number 1, 2013, Pages 27-53

# INFLUENCES OF SPRAYING PARAMETERS ON POROSITY LEVEL AND CORROSION RATE OF ATMOSPHERIC PLASMA SPRAYED ALUMINA COATINGS ON AZ31B MAGNESIUM ALLOY

**D. THIRUMALAIKUMARASAMY, K. SHANMUGAM and V. BALASUBRAMANIAN**

Department of Manufacturing Engineering
Annamalai University
Annamalainagar – 608 002
Chidambaram
Tamil Nadu
India
e-mail: tkumarasamy412@gmail.com

## Abstract

This paper reports a study of how the choice of plasma spray parameters, used during deposition of $Al_2O_3$ coatings on AZ31B magnesium alloy, influences the porosity level and corrosion rate of such coatings. The coating porosity was evaluated by using a digital image analysis method. Corrosion tests were performed for the sprayed alumina coatings in a 3.5% NaCl solution by using an immersion corrosion test. The microstructure and phase structure of the sprayed coatings were investigated by using a scanning electron microscope (SEM), X-ray diffraction (XRD), and an energy dispersive spectrometer (EDS). The results indicate that the input power has the greatest influence on porosity level and corrosion rate, followed by stand-off distance and powder feed rate.

Keywords and phrases: atmospheric plasma spraying, alumina coating, porosity, corrosion rate.

Received January 11, 2013; Revised July 29, 2013

## 1. Introduction

In moving into the 21st century, a global warming becomes a major issue all over the world. To depress the global warming, technological developments for lowering fuel consumption and reducing $CO_2$ emission are essential. A reduction in weight of materials is a means to overcome these issues. Among practical metals, magnesium is one of the lightest metals. Magnesium and its alloys have superior physical and mechanical properties, such as low density, good electromagnetic shielding, and high strength/weight ratio [1, 2]. Thus, it is strongly desired that they are applied to various transportation industries, such as the aerospace, automobile, and railway industries [3]. Their poor corrosion resistance, however, limits their use on a larger scale. Therefore, it is necessary to develop protection film to improve the anticorrosion of the magnesium alloys.

Alumina coatings are excellent candidates for providing protection against abrasive wear and resistance to galvanic and high temperature corrosion. Such coatings are desirable in electrical insulation and anti wear applications, where galvanic corrosion must be avoided, for example, in protective coatings for sleeve shafts, thermocouple jackets, electrical insulators, pump shafts, etc., and in any other application, where it is necessary to combine high resistance to wear, a low friction coefficient and high service temperatures. These coatings are usually applied using the plasma spray process, because the high temperature of the plasma flame is considered to be necessary to melt the ceramic powder particles, whereas a lower proportion of melt particles is often found when the high-velocity oxygen fuel (HVOF) technique is used [4].

Porosity is the basic and key quality characteristics to understand the microstructure and properties of thermal spray coatings. During plasma spraying, the pores and micro cracks can be generated from different sources, such as the entrapped gases, the incomplete filling in the rapidly solidifying splats, and the shrinking of the splats during

rapid solidification. If no distinction is made of the nature of pores and the micro cracks, the porosity in plasma sprayed coatings can vary from less than 2% to more than 20%, depending on the type of powders and the spray parameters used. Among these features, porosity level is a key parameter describing the anisotropy of sprayed coatings and controlling their properties. In aggressive environments, one of the major problems in using plasma sprayed coatings is the presence of the open pores, closed pores, and micro cracks in the coatings [5]. Moreover, the presence of even insignificant micro pores can substantially reduce the coating's mechanical and protective properties, such as elastic modulus, micro hardness, and bonding strength, etc.. Therefore, reduction of porosity of the sprayed coatings plays a key role in improving the corrosion resistance of the coatings.

The micro-structure and the mechanical properties of the coating are influenced by the spraying parameters, such as the spraying power, stand-off distance, and powder feed rate. These parameters influence the thermal energy and kinetic energy of particles. If particles are subjected to an excess of thermal energy, they can be vapourized in plasma jet rather than arriving at the substrate in the fully molten condition [6]. However, if the particles receive too little thermal energy, they arrive at the substrate in an unmelted condition.

Zhang et al. [7] have reported the porosity of the coating generally increased with decreasing the hydrogen gas flow rate and spraying power or increasing the powder feed rate. Celik et al. [8] studied the effect of grit blasting of substrate on the corrosion behaviour of plasma sprayed $Al_2O_3$ coatings and they identified that the corrosion resistance of the alumina coatings increased with decreasing porosity and coating thickness. Spencer et al. [9] have reported the corrosion resistance of the Al-$Al_2O_3$ composite coatings was similar to that of bulk Al alloys, and significantly better than the AZ91E Mg substrate. Toma et al. [10] studied the corrosion resistance of APS and HVOF sprayed coatings in the $Al_2O_3$-$TiO_2$ system. They observed that the corrosion resistance of

$Al_2O_3$ coatings prepared by using HVOF spraying was lower than that of the APS coatings. Dianran Yan et al. [11] investigated the corrosion behaviour of $Al_2O_3$ based ceramic composite coatings in dilute HCl solution and they found that the connected porosity in the $Al_2O_3$ based ceramic composite coatings rises with the open porosity and is independent of the density of the coating. Carboneras et al. [12] investigated the corrosion behaviour of thermally sprayed Al and Al/SiCp composite coatings on ZE41 magnesium alloy in chloride medium and they reported that the corrosion failure of these coatings is mainly related to the interconnected porosity, which is characteristic of thermally sprayed layers. The effect of APS process parameters on wear behaviour of alumina-titania coatings was investigated by Mokhtar Bounazef et al. [13].

From the literature review, it is understood that most of the published works [7-13] have focused on the corrosion and wear resistance of alumina and alumina-titania coatings. Moreover, there is no literature available related to the influences of plasma spray parameters on the porosity level and corrosion resistance of alumina coatings. Hence, in this investigation, an attempt was made to study the effect of atmospheric plasma spraying parameters on the porosity level and corrosion rate of alumina coatings on AZ31B magnesium alloy. The effect of power, stand-off distance, and powder feed rate on porosity level and corrosion rate of alumina coatings is detailed in this article.

## 2. Experimental

The chemical composition and mechanical properties of the substrate material (AZ31B magnesium alloy) are presented in Tables 1(a) and (b), respectively. The dimensions of coated specimen are shown in Figure 1. The cut sectional surface of AZ31B magnesium alloy rod (16mm in diameter and 15mm in thickness) was grit blasted by using cabinet type grit blasting machine prior to plasma spraying. Grit blasting was carried out using corundum grits of size of $500 + 320\mu m$ and subsequently

cleaned using acetone in an ultrasonic bath and dried. Plasma spraying of the alumina powder was carried out using an APS system 40kW IGBT-based Plasmatron (Make: Ion Arc Technologies; India; Model: APSS-II). The APS deposition parameters are presented in Table 2. All these parameters remained constant (Table 3), with the exception of the spraying power, stand-off distance, and powder feed rate. The feed stock was H. C. Stark, AMPERIT 740.1 powder ($Al_2O_3$) with particle size of $-45+20\mu m$. Coating thickness for all the deposits was maintained at $200 \pm 15\mu m$.

**Table 1.** (a) Chemical composition (wt%) of AZ31B Mg alloy

| Al | Mn | Zn | Mg |
|---|---|---|---|
| 3.0 | 0.20 | 1.0 | Balance |

**Table 1.** (b) Mechanical properties of AZ31B Mg alloy

| Yield strength (MPa) | Ultimate tensile strength (MPa) | Elongation (%) | Hardness (Hv) at 0.05kg load |
|---|---|---|---|
| 171 | 215 | 14.7 | 69.3 |

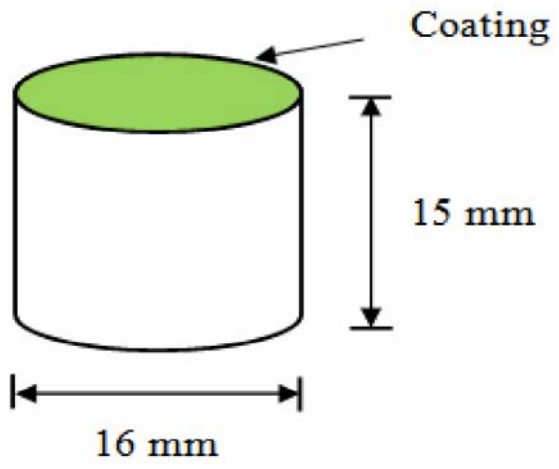


**Figure 1.** Dimensions of coated specimen.

**Table 2.** Plasma spray parameters used to coat alumina

| Process parameters | Units | Notations | Range | | | | |
|---|---|---|---|---|---|---|---|
| Power | kW | P | 18 | 20 | 22 | 24 | 26 |
| Stand-off distance | cm | S | 10 | 11 | 12 | 13 | 14 |
| Powder feed rate | gpm | F | 15 | 20 | 25 | 30 | 35 |

**Table 3.** Other relevant parameters kept constant during plasma spraying

| Parameters | Alumina coating |
|---|---|
| Plasma current (A) | 600 |
| Plasma voltage (V) | 50 |
| Primary gas flow rate(Ar) | 38 1pm |
| Secondary gas flow rate ($N_2$) | 4 1pm |

Porosity measurements were carried out on the polished cross-section of the coating as per ASTM B276 standard [14] by using optical microscope (Make: MEIJI, Japan; Model: MIL-7100) equipped with image analyzing system. The corrosion behaviour was evaluated by conducting immersion corrosion test in a 3.5% NaCl solution with a constant pH value of 7 and exposure time of 6hr. For each experimental condition, two coated specimens were prepared and tested. The edges of the coated specimens were protected by application of 45 “stopping-off” lacquer (MacDermid plc). Photographs of coated specimens before and after corrosion test are displayed in Figure 2. Corrosion rate was calculated as per the ASTM standard G31-72 [15] and evaluating the corrosion tested specimen with the method as per ASTM G1-03 [16].

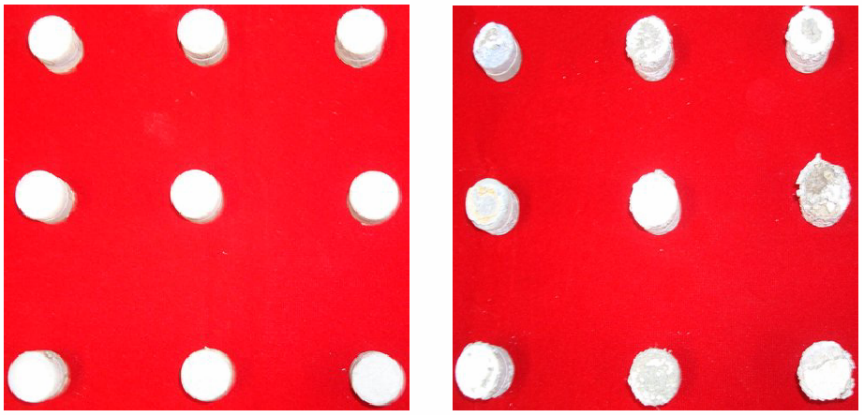

(a) Before corrosion test (b) After corrosion test

**Figure 2.** Photographs of alumina coated specimens.

### 2.1. Coating characterization

The morphologies of the powder and coating were observed with a scanning electron microscopy (Make: Quanta; Switzerland; Model: 3D FEG-I). The coatings were also subjected to SEM and EDAX analysis. The powder is fused and then crushed, which gives its characteristic angular shape with a size distribution ranging between 2-8μm as shown in Figure 3. The back scattered scanning electron micrographs of the cross-section of the alumina coating revealed the very rough surface, interconnected pores randomly distributed within the layer and poor bonding at the substrate/coating interface (Figure 4). The SEM surface morphologies of the alumina coatings on AZ31B magnesium alloy were shown in Figure 5. Spattering pattern appears on the surface, which indicates the occurrence of spraying molten drops during coating process. The alumina coatings consist of countless single spots from which a few circular pores are present on the coating surface, the non uniform growing pattern of the coating and trapping of oxygen bubbles in the coating growth process may be responsible for the extensive porosity of the ceramic coating. Further, the EDS elemental mapping results of the coating are presented in the Figure 6. From the figure, it was found that

there is no segregation of elements and the elements are uniformly distributed throughout the coating. The crystallinity of the powder and coating was measured by Philips 3121 X-ray diffractometer using CuKα radiation, which was set at 40kV and 20mA for the XRD analysis and the data were recorded in the 2θ range $10^{o}$ to $80^{o}$ in steps of $20^{o}$/min. The XRD pattern of the alumina powder exhibit α-$Al_2O_3$ phase only, whereas the XRD pattern of the sprayed coating shows both α-$Al_2O_3$ and β-$Al_2O_3$ were detected as shown in Figures 7 and 8.

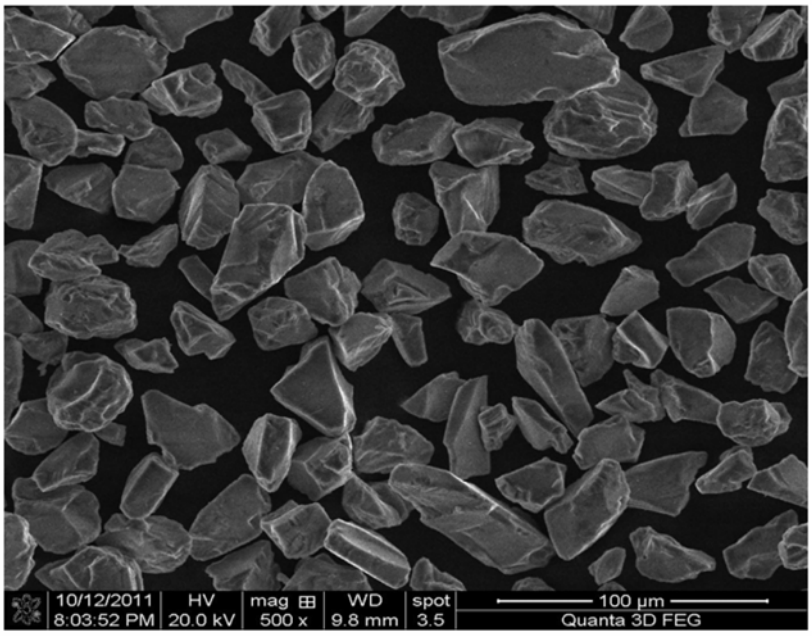


**Figure 3.** SEM micrograph of the $Al_2O_3$ powder.

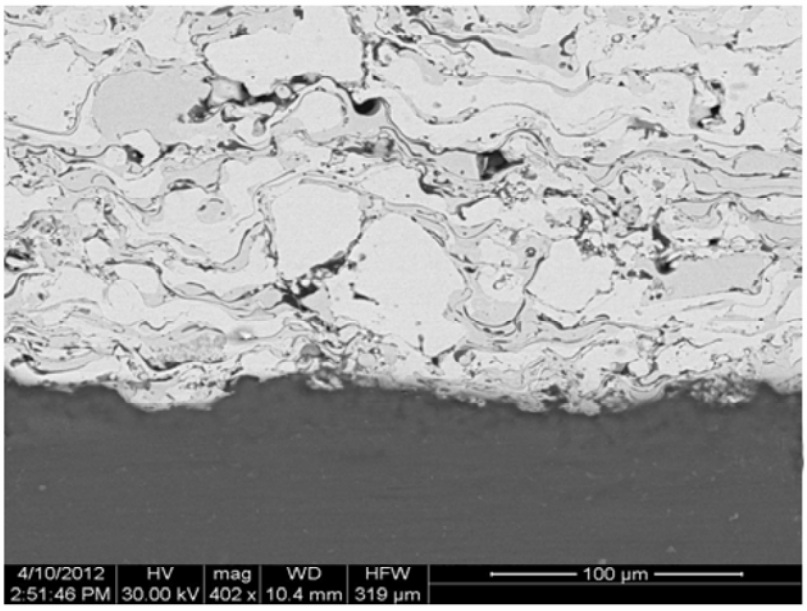


**Figure 4.** Back scattered scanning electron micrograph of the cross-section of alumina coating.

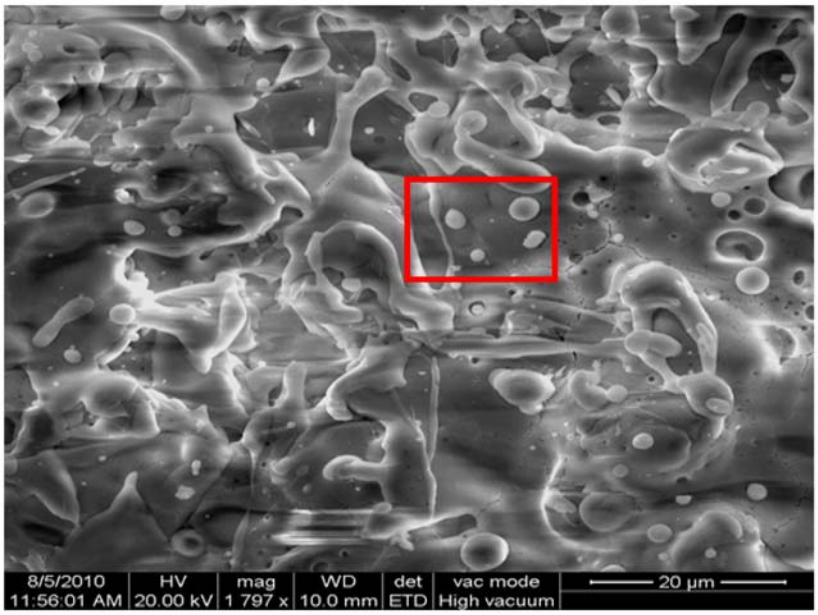


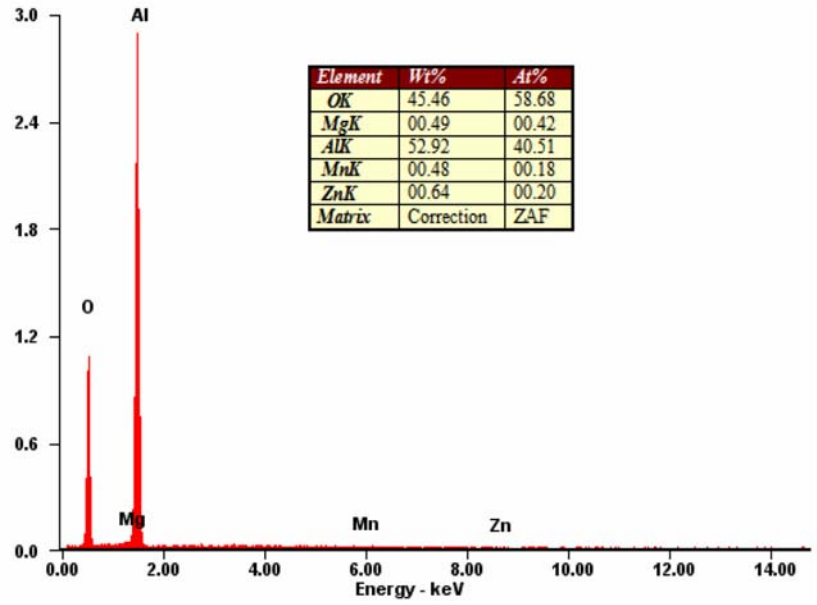


| Element | Wt% | At% |
|---|---|---|
| OK | 45.46 | 58.68 |
| MgK | 00.49 | 00.42 |
| AlK | 52.92 | 40.51 |
| MnK | 00.48 | 00.18 |
| ZnK | 00.64 | 00.20 |
| Matrix | Correction | ZAF |

**Figure 5.** SEM and EDS of $Al_2O_3$ coating.

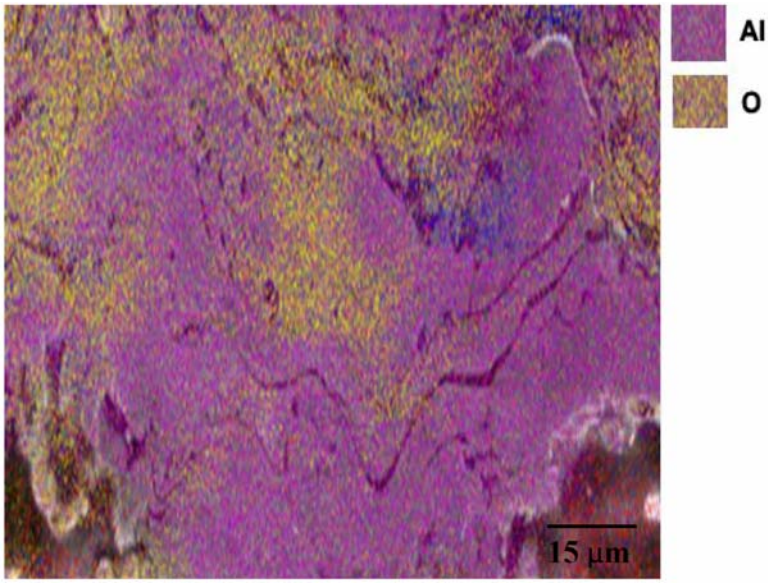


**Figure 6.** EDX mapping showing the phases elements in the coating morphology.

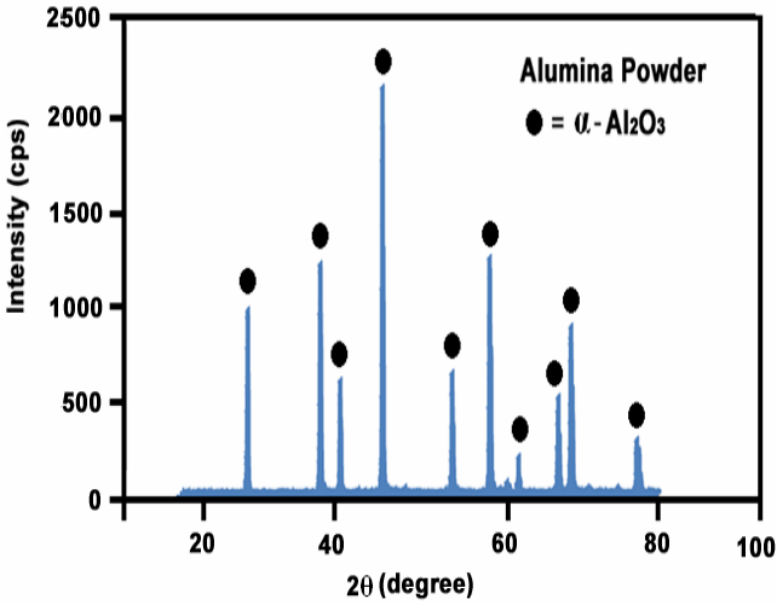


**Figure 7.** XRD pattern of the alumina powder.

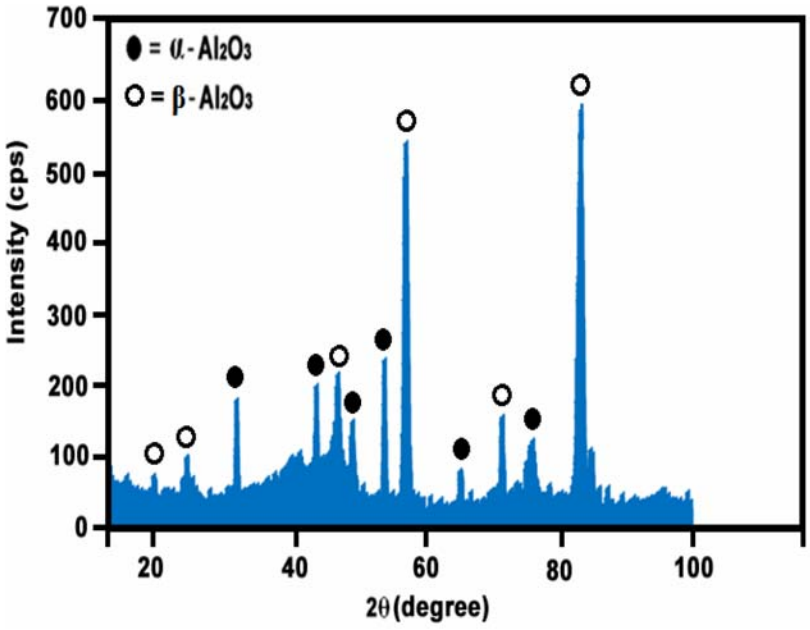


**Figure 8.** XRD pattern of the alumina coating produced by the source plasma spraying at 21.5Kw.

## 3. Results and Discussion

### 3.1. Influences of input power on porosity level and corrosion rate

The effects of input power on the porosity level and corrosion rate of the coatings are displayed in the Figure 9. From the figure, it can be inferred that, the porosity and corrosion rate decreased significantly with the increase in plasma power. $Al_2O_3$ coatings usually exhibit porosity, unmelted particles, and inclusions. It can be also observed that the coating is not so dense because of the use of an atmospheric plasma spray system, based on the pore content. The spraying power is an important parameter that affects the quality of the coating, since it can influence the temperature and velocity of the powder particles at the moment of impinging the substrate. More complete particle melting usually results in lower porosity content. At low spraying powers, the powder particles

are poorly melted. When they impact on the substrate or the already formed coating, they are not able to spread out completely to form splats and therefore, could not conform to the surface [17, 18]. In such a case, the interlamellar pores and cracks will be formed due to the solidification of the splats. Moreover, when the spraying power is relatively low, numerous unmelted and partially melted particles are existed in the coating. During the cooling process after spraying, the micro cracks and pores are formed near the boundary of the unmelted particle, since the material mismatch between the unmelted particles and the around splats, as shown in Figure 12.1(a). The poor corrosion performance of these coatings is expected to be associated with the high level of porosity of these layers allowing ready access of the aggressive solution towards the magnesium substrates, which are prone to severe corrosion in chloride containing solutions. When the power is high, the fully melted alumina due to its low melting temperature is considered to be well distributed and infiltrated in the spat boundary. When the power is sufficiently high, most of the powder particles have been melted and the flow ability of splats is good shown in Figure 12.1(b). The improved corrosion performance of $Al_2O_3$ coatings is believed to be directly associated with the elimination of interconnected pores within the layers.

Sprayed alumina coatings at high arc currents are dense with low porosity. The presence of pores inside the coatings is referred to the presence of unmelted alumina powders because the plasma power is insufficient to melt all the flight particles inside the plasma jet [19]. As the arc current increases, the plasma power increases and the heat transfer from the jet to the particles is sufficient to completely melt the powder and as a result dense coatings are formed. The corrosion rate decreases as the arc current increases because the plasma power increases and the majority of flight particles are semi or fully melted in the plasma jet before strike the substrate and forming dense structure coatings (Figure 13.1(a) and (b)).

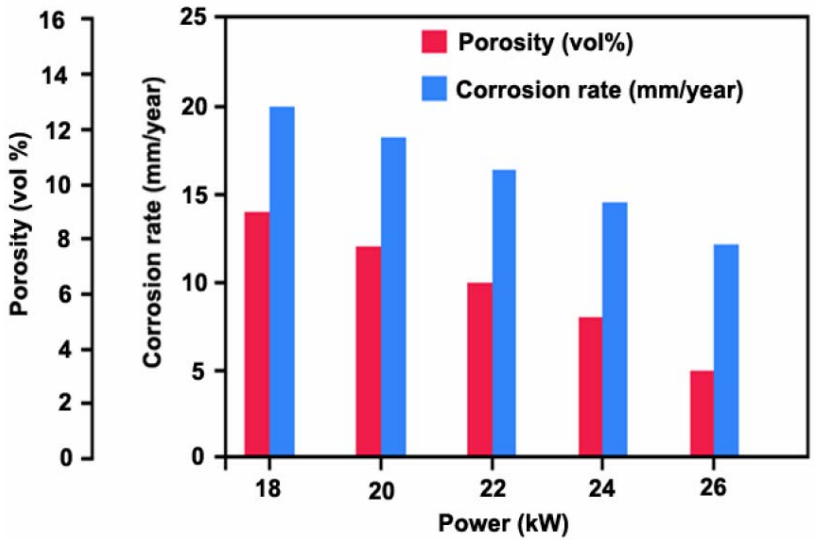


**Figure 9.** Effect of power on porosity and corrosion rate (S = 12cm, F = 25gpm).

### 3.2. Influences of stand-off distance on porosity level and corrosion rate

Figure 10 depicts the influence of the stand-off distance on the porosity and corrosion rate of the alumina coatings. It can be seen that the stand-off distance is the most important parameter affecting the porosity and corrosion rate of plasma sprayed alumina coatings. The degree of powder melting depends on the size and shape of the powder particle, and its uniform distribution. The particles pass through the plasma flame of the atmospheric plasma system and arrive in a molten form on the substrate surface. These particles solidify immediately without forming a melt pool. Therefore, the surface roughness of coatings which causes open pores usually increases corrosion rate.

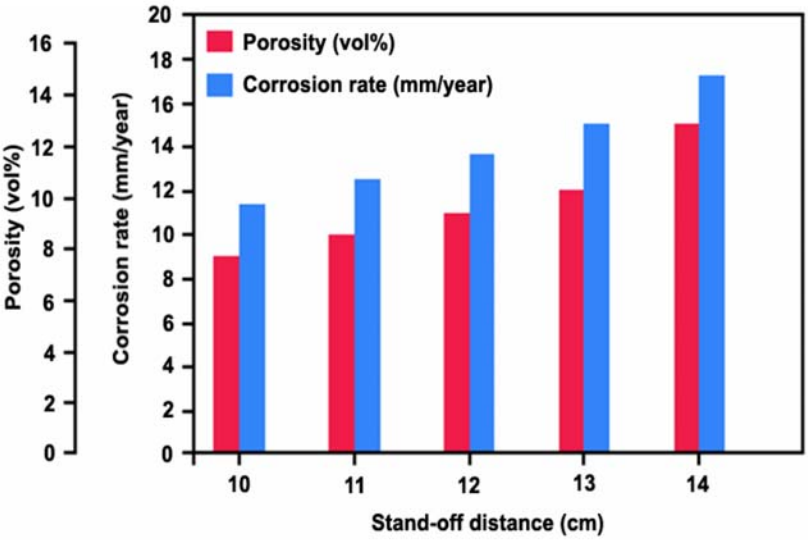


**Figure 10.** Effect of stand-off distance on porosity and corrosion rate (P = 22cm, F = 25gpm).

The crystalline of the alumina coatings increases as the spraying distance decreases mainly due to the increase of the droplet temperature at the moment of impingement. At short spraying distance, the droplets strike the substrate are semi or fully melted and as a result the alumina phase become more crystalline because the solidification rate gradually decreases as the coating thickness increases (Figure 12.2(a)). The stand-off distance mainly controls the cohesion between splats because the temperature and velocity of particles in the plasma flame significantly change with stand-off distance. Therefore, better spreading and cohesion would be achieved with shorter spraying distances [20]. A longer stand-off distance increases the probability of synthesized particle collisions, forming larger agglomerates. Since the temperature of the plasma at impact is lower at longer stand-off distance and the larger agglomerates have a higher heat capacity, the larger agglomerates would be relatively less molten, promoting the formation of coatings with higher porosity; therefore, the corrosion rate increases with the increase of stand-off distance. With a longer spray distance, the sprayed powder has more time to react with the air entrained in the flame, which would result in

an increase in oxide content with spray distance [21, 22]. It has been reported that the longer spray distance increases the dwell time in the plume and allows more thorough heating/melting of the particles. It is probable that the particle temperature will begin to decrease after a certain spray distance, as isotherms begin to decay more rapidly. This thermal processing condition results in the highest deposition efficiency and the highest hardness, while providing low levels of porosity. As can be seen from Figure 12.2(b), the corrosion resistance of plasma sprayed coating was decreased with increasing coating thickness owing to interconnected porosity, such as open pores, pinholes, and micro cracks in the film. These local defects are formed during or after spraying and act as channels providing a direct path between the corrosive environment and the substrate. In this study, NaCl solution penetrated through these channels and attacked the substrates in the form of pitting corrosion. The residual stresses increased due to increasing coating thickness. The corrosion rate of plasma sprayed $Al_2O_3$ coatings increased considerably with increasing porosity, surface roughness, and coating thickness. At shorter and longer spray distance, the particles remain unmelted or partially melted and surface roughness and corrosion rate increases (Figure 13.2(a) and (b)).

### 3.3. Influences of powder feed rate on porosity level and corrosion rate

The effect of powder feed rate on the porosity level and corrosion rate of the coatings are displayed in the Figure 11. During plasma spraying, the interaction between the gas flow and particles, the particles velocity and temperature are obviously influenced by the powder feed rate. When the powder feed rate value is low, the splats poorly flatten and spread out. There are numerous pores existing at the boundaries of overlapping splats as shown in Figure 12.3(a). Moreover, the cohesive strength between the adjacent splats is low since the micro cracks are visible at the interface. However, the greater the number of particles in the flame is, the greater the deviation from the spraying axis will be, due both to a change in the powder inlet conditions and to an increase in the opportunities for particle collisions that change the trajectories of the colliding particles [23-25]. A larger number of small and large particles

will also float on top of the flame or penetrate it to reach the lower part. It means that the injected particles are not penetrating the jet totally but are partially put aside. This could lead to improper particle heating and melting, decreasing the deposition efficiency of the spraying process due to wastage of powder. At high powder feed rate, the heat content in the plasma gas becomes insufficient for the melting of the powder particles. At the boundary of the unmelted particle, the micro cracks and pores can be found. These micro cracks and pores may be generated due to the residual stress arisen from the material mismatch of unmelted particles and the splats in a molten state. The poorly melted (unmelted and partially melted) particles will be remained in the coating, resulting in a less dense coating with high corrosion rate (Figure 12.3(b)). This behaviour is produced because as the sprayed coating is highly porous, so that, there is a high number of pathways through this coating and the electrolyte rapidly reaches the magnesium alloy surface, giving rise to the substrate corrosion as can be seen in Figure 13.3(a) and (b). This result indicates that, when the powder feed rate is high, the particles which obtain low thermal energy and kinetic energy cannot be fully melted [26-28].

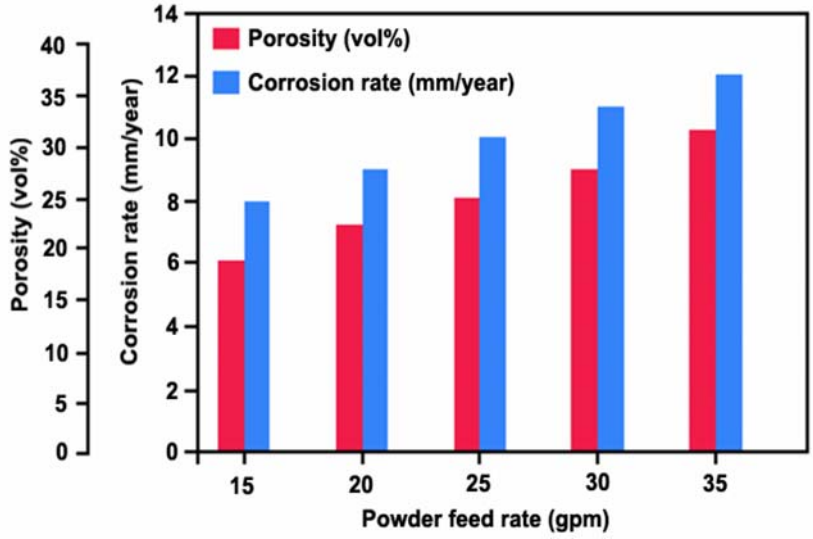


**Figure 11.** Effect of powder feed rate on porosity and corrosion rate (P = 22cm, S = 12cm).

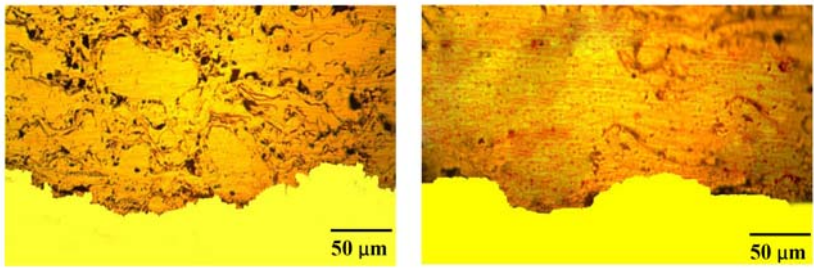


(a) 18 kW (Lowest) (b) 26 kW (Highest)

**Figure 12.1.** Effect of input power on porosity.

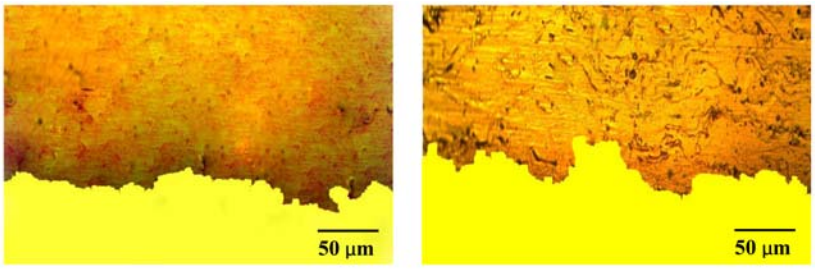


(a) 10 cm (Lowest) (b) 14 cm (Highest)

**Figure 12.2.** Effect of stand-off distance on porosity.

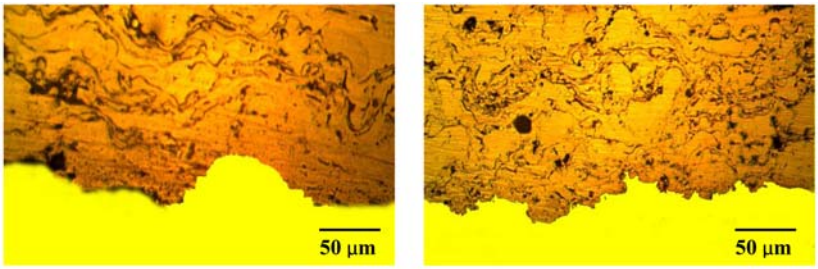


(a) 15 gpm (Lowest) (b) 35 gpm (Highest)

**Figure 12.3.** Effect of powder feed rate on porosity.

**Figure 12.** Effect of APS process parameters on porosity.

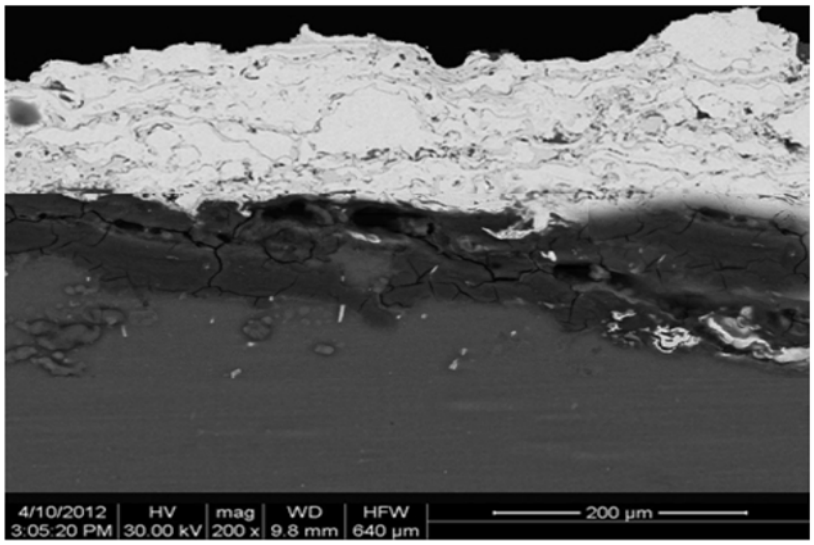


(a) 18kW (Lowest)

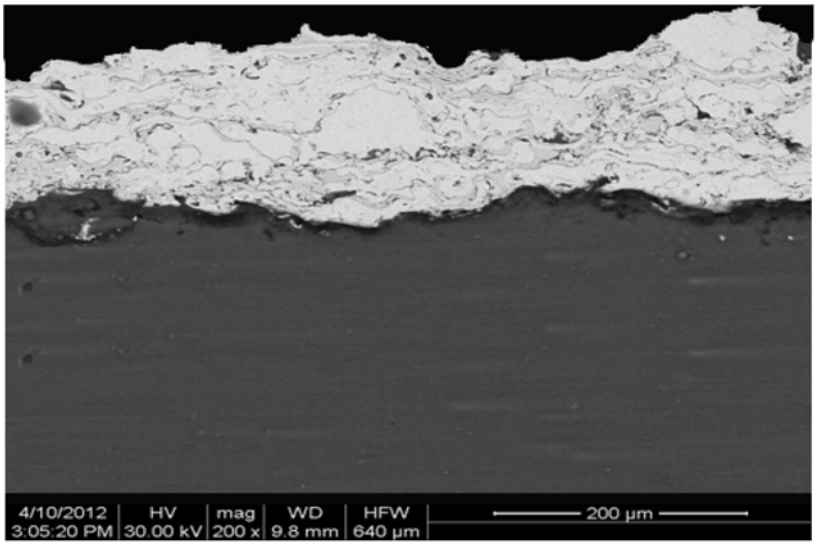


(b) 26kW (Highest)

**Figure 13.1.** Effect of input power on corrosion rate.

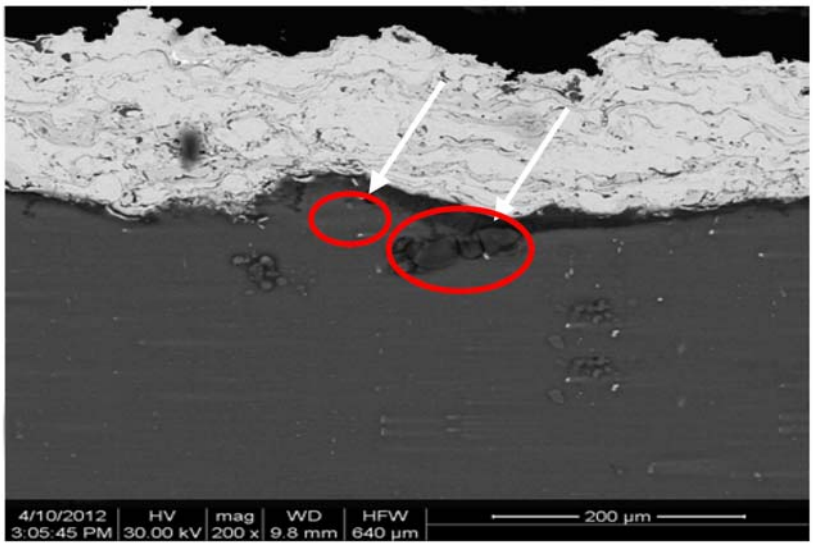


(a) 10cm (Lowest)

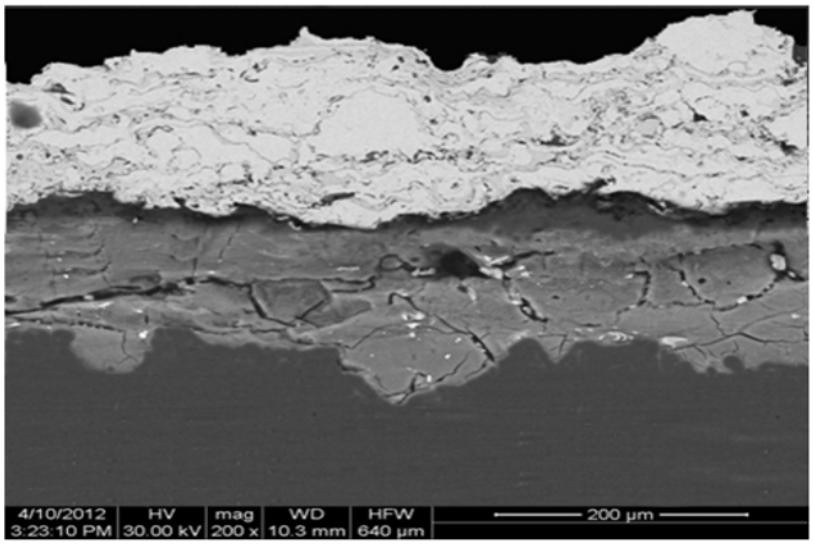


(b) 14cm (Highest)

**Figure 13.2.** Effect of stand-off distance on corrosion rate.

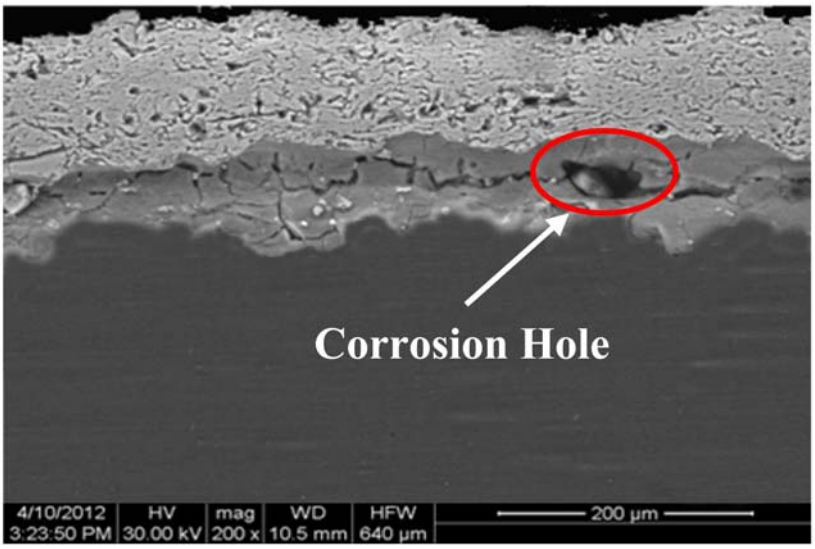


(a) 15gpm (Lowest)

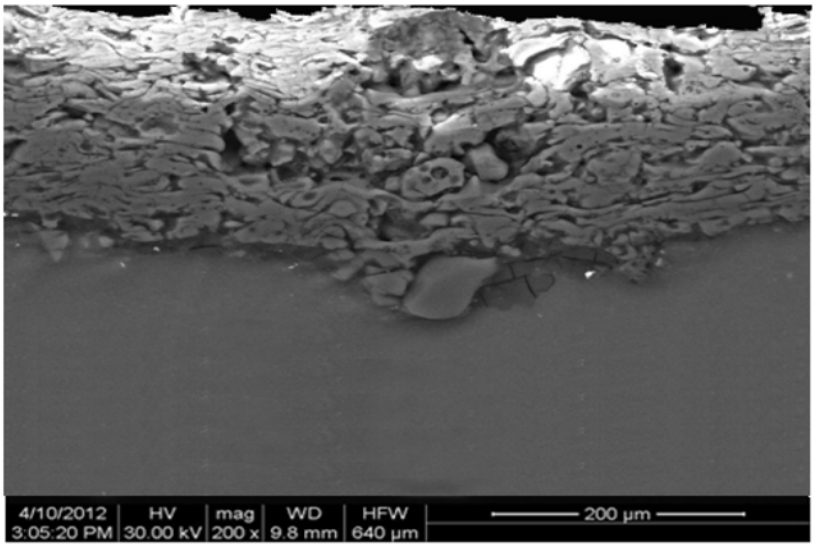


(b) 35gpm (Highest)

**Figure 13.3.** Effect of powder feed rate on corrosion rate.

**Figure 13.** Effect of APS process parameters on corrosion rate.

## 4. SEM and XRD Analysis

Figure 14 shows the SEM-EDAX results for the substrate/coating interface of alumina coating after immersion in 3.5wt% NaCl solution. From the figure, it can be inferred that corrosion attack was observed at the substrate/coating interfaces in the outermost surface of the coatings. These interfaces are known to be preferential sites for corrosion attack due to several factors, such as accumulation of defects, porosity, and discontinuity of the passive layer. EDX analysis of the corrosion products located at this interface gave an average composition of 65.3% O and 34.7% Mg (at.%), which suggested $Mg(OH)_2$ as the main corrosion product. This confirmed the presence of through pores or micro channels in the as sprayed coatings that facilitated the penetration of the aggressive medium towards the magnesium substrates. The corrosion products observed by SEM at the coating/substrate interface were not detected by the low-angle X-ray study due to the inherent limitations of this technique, however, they were probably constituted of $Mg(OH)_2$ and magnesium carbonates due to reaction of atmospheric $CO_2$ with $Mg(OH)_2$ [28]. The main corrosion products responsible for the detachment of the coatings in immersion environment were identified as $Mg(OH)_2$ (Figure 14). $Mg(OH)_2$ (brucite) has a hexagonal crystal structure and undergoes easily basal cleavage causing cracking and curling in the film.

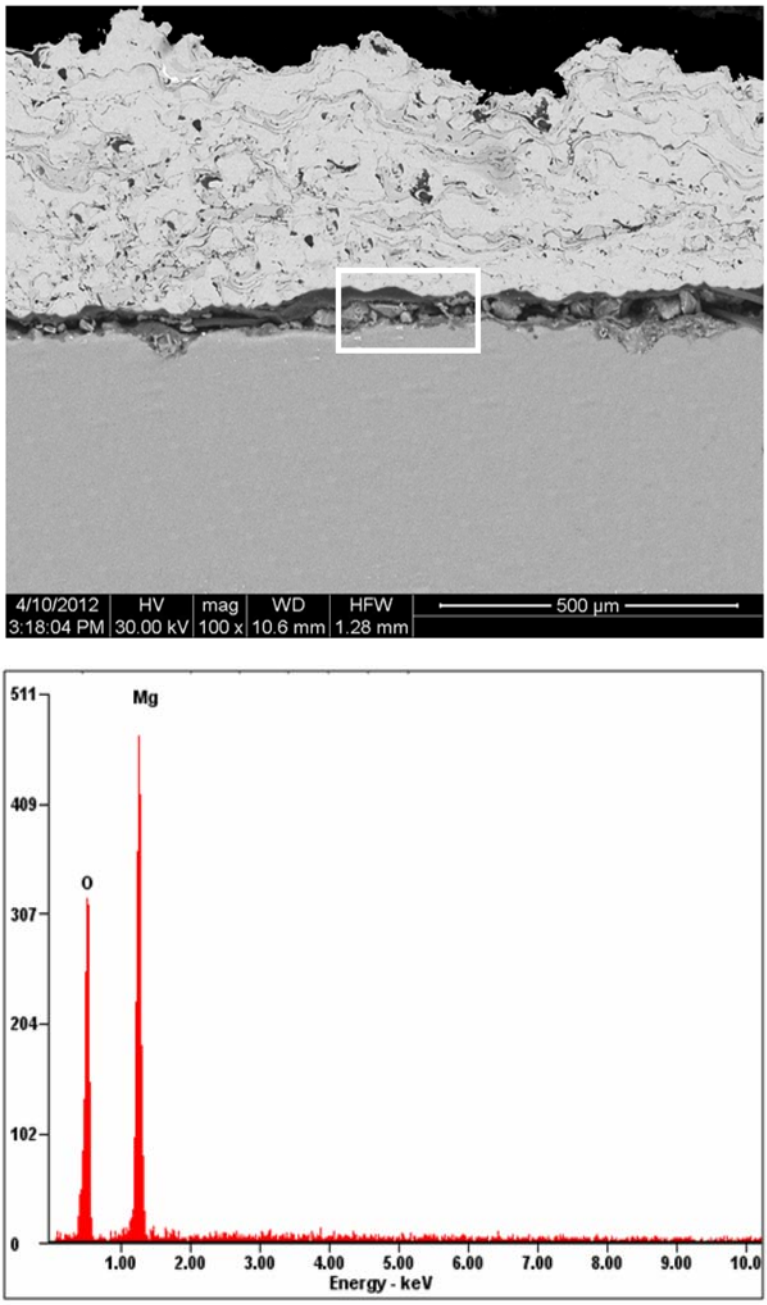


**Figure 14.** Back scattered scanning electron micrograph and EDAX of the substrate/coating interface of $Al_2O_3$ coating.

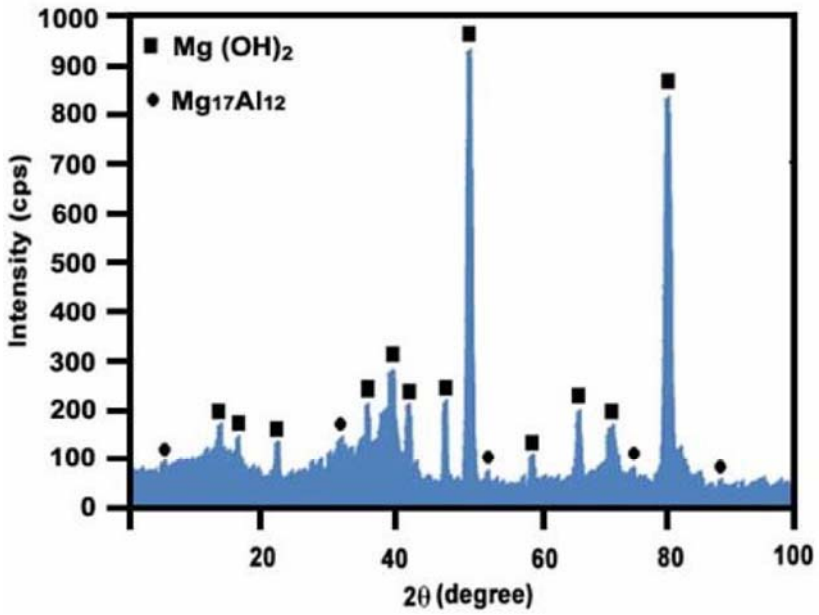


**Figure 15.** XRD study of the corrosion products formed at the substrate/coating interface of the AZ31B alloy with the $Al_2O_3$ coating after immersion corrosion test.

## 5. Conclusion

Based on the results obtained in the present study, the following main conclusions can be drawn:

- The as-sprayed alumina coatings ($Al_2O_3$-APS) revealed a poor corrosion performance in the test solution due to their high degree of interconnected pores facilitating the penetration of aggressive species towards the bulk material. Corrosion failure of these coatings is mainly related to the interconnected porosity, which is characteristic of thermally sprayed layers. Increasing the coating thickness and the energetic spraying conditions favour the reduction of porosity and improve the corrosion resistance.

● The porosity level and corrosion rate of the coatings decreased with increasing the spraying power. However, when the spraying power was sufficiently low, numerous micro cracks, pores, and many unmelted particles were observed in the coating due to the weak bonding between lamellar structures and incomplete filling in of the rapidly solidifying, etc..

● The input power has the greatest influence on porosity level and corrosion rate of the alumina coatings, followed by stand-off distance and powder feed rate.

## Acknowledgement

The authors wish to express their sincere thanks to Dr. C. S. Ramachandran, Project Officer, the Department of Manufacturing Engineering, Annamalai University, for the help rendered during deposition of the coatings. The authors also wish to thank Mr. R. Selvendiran, Technical Assistant, Cemajor, Annamalai University for his help in carrying out this investigation. The technical support of Dr. R. Paventhan, Professor and Head, JJ College of Engineering and Technology, Trichirappalli, during the course of this work is gratefully acknowledged.

## References

[1] W. C. Neil, M. Forsyth, P. C. Howlettt, C. R. Hutchison and B. R. W. Hinton, Corrosion of magnesium alloy ZE41 : The role of micro-structural features, Corrosion Science 51 (2009), 387-394.

[2] Lei Wang, Bo-Ping Zhang and Tadashi Shinohara, Corrosion behaviour of AZ91 magnesium alloy in dilute NaCl solutions, Materials and Design 31 (2010), 857-863.

[3] B. L. Mordike and T. Ebert, Magnesium: Properties, applications, potential, Mater. Sci. Eng. A 302 (2001), 37.

[4] N. Krishnamurthy, M. S. Murali, B. Venkataraman and P. G. Mukunda, Characterization and solid particle erosion behaviour of plasma sprayed alumina and calcia-stabilized zirconia coatings on Al-6061 substrate, Wear 274-275 (2012), 15-27.

[5] L. Wang, J. C. Fang, Z. Y. Zhao and H. P. Zeng, Application of backward propagation network for forecasting hardness and porosity of coatings by plasma spraying, Surf. Coat. Technol. 201 (2007), 5085-5089.

[6] X. C. Zhang, B. S. Xu, F. Z. Xuan, H. D. Wang , Y. X. Wu and S. T. Tu, Statistical analyses of porosity variations in plasma-sprayed Ni-based coatings, J. Alloys Compd. 467 (2009), 501-508.

[7] X. C. Zhang, B. S. Xu, F. Z. Xuan, H. D. Wang and Y. X. Wu, Microstructural and porosity variations in the plasma-sprayed Ni-alloy coatings prepared at different spraying powers, Journal of Alloys and Compounds 473 (2009), 145-151.

[8] E. Celik, I. Ozdemir, E. Avci and Y. Tsunekawa, Corrosion behaviour of plasma sprayed coatings, Surface & Coatings Technology 193 (2005), 297-302.

[9] K. Spencer, D. M. Fabijanic and M. X. Zhang, The use of Al-$Al_2O_3$ cold spray coatings to improve the surface properties of magnesium alloys, Surf. Coat. Technol. 204 (2009), 336-344.

[10] F. L. Toma, C. C. Stahr, L. M. Berger, S. Saaro, M. Herrmann, D. Deska and G. Michael, Corrosion resistance of APS and HVOF sprayed coatings in the $Al_2O_3$-$TiO_2$ system, J. Thermal Spray Technol. 19 (2009), 137-147.

[11] Dianran Yan, Jining He, Xiangzhi Li, Yangaia Liu, Jianxin Zhang and Huili Ding, An investigation of the corrosion behaviour of $Al_2O_3$ based ceramic composite coatings in dilute HCl solution, Surface and Coatings Technology 141 (2001), 1-6.

[12] M. Carboneras, M. D. Lopez, P. Rodrigo, M. Campo, B. Torres, E. Otero and J. Rams, Corrosion behaviour of thermally sprayed Al and Al/SiCp composite coatings on ZE41 magnesium alloy in chloride medium, J. Corros. Sci. 52 (2010), 761-768.

[13] Mokhtar Bounazef, Sofiane Guessasma, Ghislain Montavon and Christian Coddet, Effect of APS process parameters on wear behaviour of alumina-titania coatings, Materials Letters 58 (2004), 2451-2455.

[14] ASTM B276-05, Standard Test Method for Apparent Porosity in Cemented Carbides, Pennsylvania: American Society for Testing and Materials, 2010, Volume 02-05.

[15] ASTM G31-72, Standard Practice for Laboratory Immersion Corrosion Testing of Metals, American Society for Testing of Materials, 2002.

[16] ASTM G1-03, Standard Practice for Preparing, Cleaning and Evaluating Corrosion Test Specimens, American Society for Testing of Materials, 2003.

[17] You Wang, Wei Tian, Tao Zhang and Yong Yang, Microstructure, spallation and corrosion of plasma sprayed $Al_2O_3$-13%$TiO_2$ coatings, Corrosion Science 51 (2009), 2924-2931.

[18] Heng Wu, He-jun Li, Qing Lei, Qian-gang Fu, Chao Ma, Dong-jia Yao, Yong-jie Wang, Can Sun, Jian-feng Wei and Zhi-hai Han, Effect of spraying power on microstructure and bonding strength of $MoSi_2$-based coatings prepared by supersonic plasma spraying, Journal of Applied Surface Science 257 (2011), 5566-5570.

[19] R. Arrabal, A. Pardo, M. C. Merino, M. Mohedano, P. Casajus and S. Merino, Al/SiC thermal spray coatings for corrosion protection of Mg-Al alloys in humid and saline environments, Surface & Coatings Technology 204 (2010), 2767-2774.

[20] A. Pardo, P. Casajus, M. Mohedano, A. E. Coy, F. Viejo, B. Torres and E. Matykina, Corrosion protection of Mg/Al alloys by thermal sprayed aluminium coatings, Applied Surface Science 255 (2009), 6968-6977.

[21] C. S. Ramachandran, V. Balasubramanian and P. V. Ananthapadmanabhan, Multiobjective optimization of atmospheric plasma spray process parameters to deposit yttria-stabilized zirconia coatings using response surface methodology, J. Therm. Spray. Technol. 20 (2010), 590-607.

[22] A. Kucuk, C. C. Berndt, U. Senturk, R. S. Lima and C. R. C. Lima, Influence of plasma spray parameters on mechanical properties of yttria-stabilized zirconia coatings, I: Four point bend test, Mater. Sci. Eng. A 284 (2000), 29-40.

[23] Yongshan Tao, Tianying Xiong, Chao Sun, Lingyan Kong, Xinyu Cui, Tiefan Li and Guang-Ling Song, Microstructure and corrosion performance of a cold sprayed aluminium coating on AZ91D magnesium alloy, Corrosion Science 52 (2010), 3191-3197.

[24] C. S. Ramachandran, V. Balasubramanian and P. V. Ananthapadmanabhan, On resultant properties of atmospheric plasma sprayed yttria-stabilised zirconia coating deposits: Designed experimental and characterisation analysis, Surf. Eng. 27 (2011), 217-229.

[25] Jifu Zhang, Wei Zhang, Chuanwei Yan, Keqin Du and Fuhui Wang, Corrosion behaviours of Zn/Al-Mn alloy composite coatings deposited on magnesium alloy AZ31B (Mg-Al-Zn), Journal of Electrochimica Acta 55 (2009), 560-571.

[26] Wei-min Zhao, Cun Liu, Li-xian Dong and Yong Wang, Effects of arc spray process parameters on corrosion resistance of Ti coatings, Journal of Thermal Spray Technology 518 (2009), 702-707.

[27] L. Gil and M. H. Staia, Influence of HVOF parameters on the corrosion resistance of NiWCrBSi coatings, Journal of Thin Solid Films 420 (2002), 446-454.

[28] V. Balasubramanian, A. K. Lakshminarayanan, R. Varahamoorthy and S. Babu, Understanding the parameters controlling plasma transferred arc hard facing using response surface methodology, Materials and Manufacturing Processes 23 (2008), 674-682.

■